GEOLOGY | THE GEOLOGICAL SOCIETY OF AMERICA®

https://doi.org/10.1130/G45542.1

Manuscript received 30 August 2018
Revised manuscript received 1 November 2018
Manuscript accepted 6 November 2018

Published online 30 November 2018

Upper mantle origin of plagioclase megacrysts from plagioclase-ultraphyric mid-oceanic ridge basalt

Mélissa J. Drignon[1], Roger L. Nielsen[1], Frank J. Tepley III[1], and Robert J. Bodnar[2]
[1]College of Earth, Ocean and Atmospheric Science, Oregon State University, Corvallis, Oregon 97331, USA
[2]Department of Geosciences, Virginia Tech, Blacksburg, Virginia 24061, USA

ABSTRACT

Rigorous petrogenetic interpretation of data from melt inclusions (MI) and their host phenocrysts commonly requires knowledge of the crystallization pressure. Pressures of trapping of MI are commonly estimated based on the H_2O and CO_2 concentrations of the inclusions, but their original concentrations may be modified as a result of various post-entrapment processes. Most studies of mafic magmas employ olivine- or pyroxene-hosted MI, largely based on the assumption that plagioclase phenocrysts do not retain volatiles and/or are the product of late-stage crystallization. We have investigated the effects of post-entrapment processes on plagioclase-hosted MI in one plagioclase-ultraphyric basalt from the Blanco transform fault (offshore Oregon, USA). Our results demonstrate that plagioclase-hosted MI do not lose CO_2 even after being heated to the entrapment temperature for 4 d. The reconstructed CO_2 (glass + vapor) concentration in the MI indicates that the plagioclase megacrysts crystallized at depths equal to or below the local Moho, at minimum pressures of 230–910 MPa. Our results confirm that the plagioclase crystallized in the mantle, and that reliable trapping pressures can be obtained from MI in plagioclase following rehomogenization experiments.

INTRODUCTION

Plagioclase is a common phenocryst phase in mid-ocean ridge basalts (MORBs) and is assumed to crystallize later than olivine in the differentiation sequence (Bryan, 1983). Therefore, most work on melt inclusions (MI) in MORBs aimed at understanding the early crystallization history has focused on olivine (e.g., Wanless and Shaw, 2012; Le Voyer et al., 2017). In addition, it has been commonly assumed that MI in plagioclase are susceptible to leakage and do not preserve the primary volatile concentration. However, little evidence exists to support the contention that plagioclase-hosted MI are more susceptible to $CO_2 + H_2O + S$ loss compared to MI in olivine.

This study focuses on plagioclase-hosted MI from a single plagioclase-ultraphyric basalt (PUB) from the Blanco transform fault (offshore Oregon, USA). PUBs are characterized by >15 modal% anorthitic plagioclase megacrysts (Lange et al., 2013). The megacrysts are commonly xenocrystic, but their host glasses usually show a chemistry that is similar to that of the array of erupted lavas from their ridge segment. The plagioclase megacrysts and their MI are usually more primitive (more An and Mg rich) and compositionally more diverse than late-crystallizing plagioclase crystals that are in equilibrium with their associated lavas near the surface (Lange et al., 2013; Neave et al., 2014).

The H_2O-CO_2 concentrations of MI can be related to pressures of trapping through solubility models, and therefore can give useful information on the crystallization pressures of the plagioclase megacrysts (Dixon et al., 1995; Newman and Lowenstern, 2002). Most existing pressure estimates are from olivine-hosted MI in MORBs and are consistent with crystallization within the oceanic crust, with a minority indicative of deeper mantle crystallization (Wanless and Shaw, 2012; Wallace et al., 2015; Le Voyer et al. 2017., Wanless and Behn, 2017). Fewer studies have utilized plagioclase-hosted MI to determine the pressure of crystallization (Helo et al., 2011; Coumans et al., 2015; Neave et al., 2015, 2017). However, those studies reported entrapment pressures as high as, or higher than, those obtained from olivine-hosted MI.

Determining the pressure at which the melt was trapped based on H_2O-CO_2 concentrations of MI is complicated by the fact that most MI contain a vapor bubble at room temperature, and some of the originally trapped CO_2 is contained in the melt (glass) and some is in the vapor bubble (Steele-MacInnis et al., 2011; Hartley et al., 2014; Moore et al., 2015). Calculations of pressures of trapping of the MI thus requires knowledge of the amounts of CO_2 and H_2O in the melt (glass) and in the vapor bubble. Our aim in this study is to assess whether pressures calculated from plagioclase-hosted MI are dependent on the duration of heating experiments to homogenize the contents of the MI.

GEOLOGICAL SETTING AND METHODOLOGY

PUBs are found worldwide at slow- and intermediate-spreading centers, as well as at off-axis seamounts and transform faults where the absence of a magma reservoir may inhibit crystals from being filtered out of their host magmas (Lange et al., 2013). We focus on the Blanco transform fault, a right-lateral transform fault zone that extends for >360 km and separates the Juan de Fuca Ridge to the northwest from the Gorda Ridge to the southeast (Embley and Wilson, 1992). We examined megacrysts from a single sample (A91-1R) collected at 44°12.55′N, 129°37.93′W (Embley and Wilson, 1992) that is characterized by abundant (~20%) euhedral, centimeter-scale (0.2–1 cm) plagioclase megacrysts. Plagioclase crystals from this sample are unzoned and have a narrow range of anorthite contents ($An_{[83 \pm 2]}$). PUB megacrysts show Sr isotopic signatures that are similar to those of their host lavas (Lange et al., 2013). Experiments performed on high-An plagioclase revealed that MI are trapped during an isothermal period of growth during which fast diffusion prevented the development of boundary layers (Kohut and Nielsen, 2004).

The naturally quenched MI in our samples are fully or partially crystallized by post-entrapment crystallization and contain one or multiple vapor bubbles, making experimental homogenization before analysis a necessity (Fig. DR1

CITATION: Drignon, M.J., Nielsen, R.L., Tepley F.J., III, and J. Bodnar, R.J.,, 2018, Upper mantle origin of plagioclase megacrysts from plagioclase-ultraphyric mid-oceanic ridge basalt: Geology, v. 47, p. 43–46, https://doi.org/10.1130/G45542.1.

in the GSA Data Repository[1]). We performed homogenization experiments at Oregon State University (Corvallis, Oregon, USA) using a 0.1 MPa vertical furnace. Individual crystals were suspended in the furnace at 1230 °C for 30 min or 4 d and quenched (see Appendix DR1 in the Data Repository for more information). The crystals were then polished to expose the MI for Raman and secondary ionization mass spectrometry (SIMS) analyses. Raman analyses were performed at Virginia Tech (Blacksburg, Virginia, USA) to determine the density of CO_2 within the vapor bubbles. Then, the same MI were analyzed at Woods Hole Oceanographic Institution (WHOI, Woods Hole, Massachusetts, USA) by SIMS to determine the CO_2, H_2O, S, Clc and F concentrations within the glass phase of the MI. The total CO_2 concentration in each MI was reconstructed by combining the CO_2 from the vapor bubble and CO_2 from the glass (Moore et al., 2015). We used VolatileCalc 2.0 software (Newman and Lowenstern, 2002) to estimate the minimum trapping pressures based on the H_2O-CO_2 concentrations of the MI. We computed H_2O-CO_2 concentrations for 27 MI from eight crystals that were homogenized for 30 min, and for 16 MI from eight crystals that were homogenized for 4 d. Additional information of the methodology used can be found in Appendix DR1.

TABLE 1: COMPARISON OF VOLATILE CONTENTS AND ENTRAPMENT ESTIMATES OF MELT INCLUSIONS FOR TWO EXPERIMENTAL RUN TIMES

	30 min	4 d
CO_2 total (ppm)	2253 ± 800	2714 ± 1183
S glass (ppm)	821 ± 100	671 ± 179
Cl glass (ppm)	36 ± 12	55 ± 63
F glass (ppm)	20 ± 15	0.73 ± 0.28
Pressure (MPa)	409 ± 118	473 ± 152
Depth (km)	12 ± 3	14 ± 5
CO_2 in bubble (%)	71 ± 14	83 ± 10
Number of analyses	27	16

Note: Averages with 1σ errors (standard deviation) of the volatiles analyzed for both experimental run times within the glass of the melt inclusions (MI) by secondary ionization mass spectrometry: H_2O in wt%; S, Cl, and F in ppm. Total CO_2 (ppm) represents the calculated CO_2 in the MI, combining the CO_2 concentrations of the glass and vapor bubbles, together with volume estimates for both. The averaged pressures and depths calculated using VolatileCalc2.0 (Newman and Lowenstern, 2002) are also shown, as well as the percentage of total CO_2 present in the vapor bubbles of the MI, and the number of MI analyzed for both run times.

RESULTS

The reconstructed CO_2 concentrations of MI held at 1230 °C for 30 min average 2253 ± 800 ppm CO_2 (1σ), and average 2714 ± 1183 ppm CO_2 for the 4 d runs (Table 1). The melts are anhydrous, with <0.1 wt% H_2O detected in MI from both runs. Calculated minimum crystallization pressures yielded similar results for both run times, with no systematic difference between MI in different crystals. The 30 min runs yield an average pressure of 409 ± 118 MPa (1σ), and the 4 d runs yield an average of 473 ± 152 MPa (Table 1; Fig. 1). The uncertainties on these values reflect sample variability rather than uncertainty in the solubility model. Our results show that 71% ± 14% (1σ) of the CO_2 is in the vapor bubbles after the 30 min run, whereas 83% ± 10% of the CO_2 is in the vapor bubbles after the 4 d runs (Table 1). It is important to note here that >50% of the CO_2 is typically present within the vapor bubbles for both run times (Table DR1 in the Data Repository), highlighting the importance of analyzing vapor bubbles for CO_2 to determine the original volatile content of the trapped melt, as has been reported by Moore et al. (2015). Unpaired *t*-test calculations for both the total reconstructed CO_2 and the CO_2 distribution revealed that: (1) the total reconstructed CO_2 is not statistically different for the 30 min and 4 d runs; and (2) the CO_2 distribution within vapor bubbles is statistically different between the two experimental run times, with a relatively larger proportion of the total CO_2 contained in the vapor bubble for the 4 d runs (Table DR2).

The behavior of other volatile components varied between the two runs, with 821 ± 100 ppm S (1σ) for the 30 min runs, and 671 ± 179 ppm S for the 4 d runs (Table 1). According to Wallace and Carmichael (1992), all MORB magmas are sulfide saturated. As such, any MI that lie off of the sulfide saturation line are assumed to have been compromised and to have lost sulfur (and other volatiles). Only MI that lie on the sulfide saturation line were included in this study. Similarly, the F concentration in the 30 min runs averages 20 ± 15 ppm (1σ) but is below the detection limit of 1.8 ppm for the 4 d runs (Table 1; Fig. 2). It is not clear if F diffused out of the MI during the 4 d runs or if it exsolved from the melt and into the vapor bubbles (Koleszar et al., 2009). Unlike S and F, Cl concentrations are identical within error for the two run times, with 36 ± 12 ppm and 55 ± 63 ppm (1σ), respectively, for the 30 min and the 4 d runs.

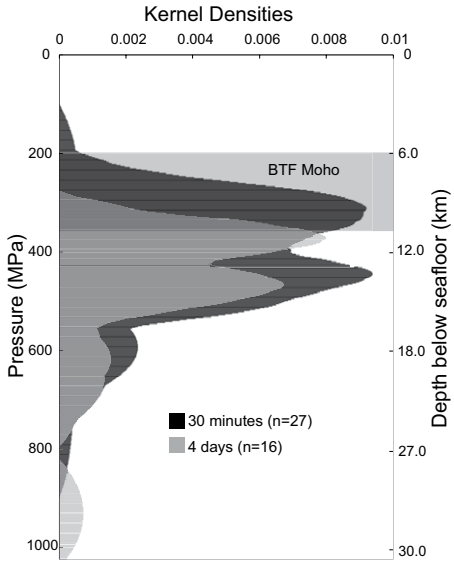

Figure 1. Kernel density plot of pressures calculated for melt inclusions (MI) heated for 30 min (black) and for 4 d (gray). Kernel density plots represent probability density functions for which distribution parameters are unspecified. Pressures were calculated using VolatileCalc 2.0 software (Newman and Lowenstern, 2002) using measured H_2O concentration from secondary ionization mass spectrometry and total reconstructed CO_2 for each MI (Newman and Lowenstern, 2002; Moore et al., 2015). 2σ errors were computed with kernel density plots. Moho pressures in gray are from McNutt (1979) and Christeson et al. (2010). Number of MI plotted (*n* = *x*) is noted in legend. BTF—Blanco transform fault (offshore Oregon, USA).

DISCUSSION

Impact of Post-Entrapment Processes on the Volatile Concentrations of MI

Diffusive Loss of Hydrogen

All of the MI studied exhibit low H_2O concentrations, which may be attributed to diffusive loss of H and/or a low initial H_2O content (Métrich and Wallace, 2008). Johnson and Rossman (2013) reported an increase in OH loss with increasing run time and temperature in experiments using An_{30} plagioclase. Assuming that the MI originally contained little H_2O (<~1 wt%), loss of H_2O from the MI would have little influence on the pressure estimates because the H_2O-CO_2 saturation pressure isobars are essentially independent of H_2O at concentrations of ≤0.5 wt% (Gaetani et al., 2012).

[1]GSA Data Repository item 2019010, Figure DR1 (BSE images of MI prior to and post-rehomogenization experiments), Figure DR2 (graph of Mg# versus % crystallization for both run times), Table DR1 (details of the volatile content and pressure and depth of entrapment for each MI analyzed),Table DR2 (unpaired *t*-test results), and Table DR3 (details of Mg#, MgO, FeO, F parameter, and % crystallization for each MI), is available online at http://www.geosociety.org/datarepository/2019/ or upon request from editing@geosociety.org.

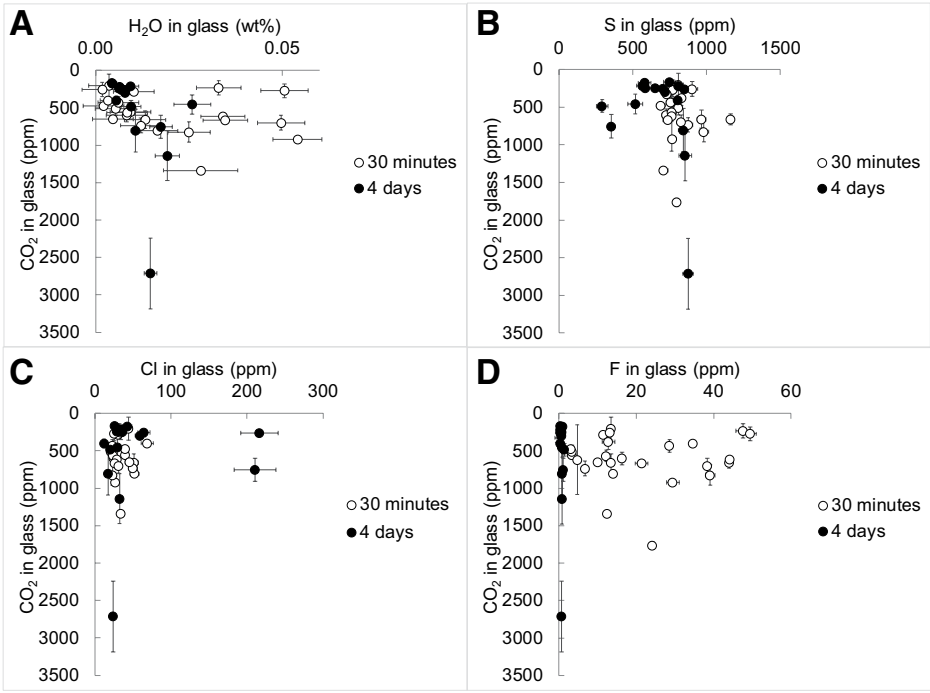

Figure 2. Volatile contents of glass phase in melt inclusions (MI). Open circles are MI held at 1230 °C for 30 min; solid black circles are MI held at 1230 °C for 4 d. 1σ error bars are calculated for each analysis. All data are plotted against CO_2 (ppm) in glass on *y*-axis. A: H_2O (wt%) in glass phase in MI. B: Sulfur (ppm) in glass phase in MI. C: Chlorine (ppm) in glass phase in MI. D: Fluorine (ppm) in glass phase in MI. Errors are consistent with those determined previously during rigorous assessment of uncertainties associated with analyses of volatiles in MI using same analytical methods and instrumentation (Esposito et al., 2014).

Leakage

Leakage of volatiles such as CO_2 results in lower CO_2 concentrations in the MI, and this, in turn, could lead to a possible incorrect interpretation that the MI trapped a volatile-undersaturated melt (Maclennan, 2017). Leakage is more likely for volatile-rich MI with high internal pressure (Bodnar, 2003; Maclennan, 2017; Wanless and Behn, 2017). In CO_2-rich and H_2O-poor systems, the formation of vapor bubbles induces an internal pressure decrease, thus minimizing the probability that the MI will leak.

Vapor Bubbles

Vapor bubbles can form as a result of cooling of MI and post-entrapment crystallization, leading to volatile exsolution from the melt (Kent, 2008). All of the MI studied here contained one or more vapor bubbles. As noted above, >50% of the CO_2 is present in vapor bubbles for both experimental run times. In addition, the MI heated for 4 d likely experienced compositional changes that could impact the solubility of CO_2 because the solubility of CO_2 decreases with decreasing CaO, MgO, and alkaline contents (Brey, 1976; Moore, 2008).

Crystal Relaxation

Schiavi et al. (2016) demonstrated that crystal relaxation occurs when a crystal is maintained at elevated temperature for long times at 1 atm confining pressure. Crystal relaxation occurs because at high temperature, the internal pressure in volatile-rich MI is much greater than the 0.1 MPa confining pressure on the crystal host, leading to a large pressure differential. When the MI in this study are heated to 1230 °C, the pressure in the MI reaches several hundreds of megapascals, and the plagioclase host surrounding the MI relaxes over a period of days to eliminate the pressure gradient between the MI and surrounding plagioclase host. During relaxation the MI volume increases and the internal pressure in the MI decreases, inducing further CO_2 exsolution into the vapor bubbles. This interpretation is supported by the increased density of CO_2 in the vapor bubbles after the 4 d runs compared to the 30 min runs (Fig. 3).

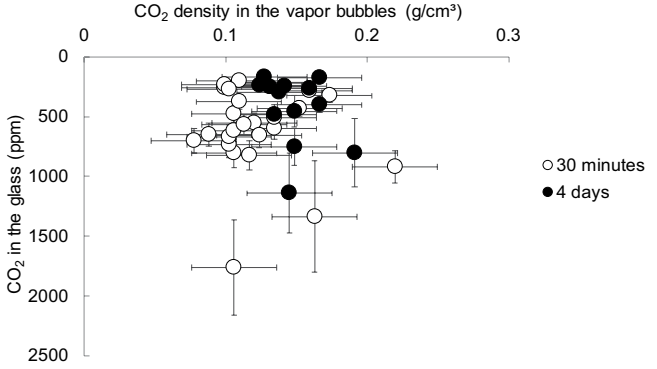

Figure 3. CO_2 in glass phase determined by secondary ionization mass spectrometry versus density of CO_2 in vapor bubbles (g/cm³) determined by Raman analysis for 30 min runs (open circles) and 4 d runs (black circles). 2σ errors are also shown.

On the Mantle Origin of Sample A91-1R

The oceanic crust under the Blanco transform fault is ~6.7–10.0 km thick based on seismic imaging (McNutt, 1979; Christeson et al., 2010). The samples analyzed in this study yield a range of CO_2 concentrations that indicate minimum pressures ranging from 230 to 910 MPa, corresponding to depths of 6–27 km, all of which are at or below the local Moho (Fig. 1; Table DR1). In contrast, most pressures calculated based on MORB glasses and olivine-hosted MI compositions indicate that the olivine phenocrysts formed in the mid-crust, with a minority at deeper levels (e.g., Wanless and Shaw, 2012; Wallace et al., 2015; Wanless and Behn, 2017). Previous studies of plagioclase-hosted MI in MORBs recorded both crustal (Neave et al., 2015, 2017) and mantle depths (Helo et al., 2011; Coumans et al., 2015). Current models for the formation of PUBs involve plagioclase crystallization in the upper mantle and interaction of melts with troctolitic cumulates during magma ascent (Kohut and Nielsen, 2003; Lange et al., 2013). MORB melts can entrain high-anorthite plagioclase in the upper mantle due to their similar density (~2.7 g/cm³). During ascent, the melts become less dense than the plagioclase crystals, which can only be erupted if the ascent rate is greater than the settling rate. The density contrast between olivine (3.2 g/cm³) and plagioclase would result in crystal sorting and the eruption of PUBs containing little or no olivine. Therefore, our mantle pressure estimates are consistent with the model of PUB formation conceptualized by Kohut and Nielsen (2003) and Lange et al. (2013). In addition, the mantle origin of our sample is supported by the near-primary compositions of the MI (Mg# of 67.53 ± 2.48 [2σ]; Michael and Graham, 2015; Appendix DR2; Fig. DR2; Table DR3).

CONCLUSIONS

We have documented that plagioclase-hosted MI retain their original CO_2 concentrations, even after being held at 1230 °C for 4 d. However, during these experiments conducted at 1 atm pressure, crystals underwent time-dependent relaxation, resulting in expansion of the plagioclase hosts and an increase in the volume

of their contained MI. The resulting pressure decrease within the MI and the concomitant decrease in CO_2 solubility led to the exsolution of CO_2 from the melt and into the vapor bubbles. However, the total CO_2 concentrations in the MI, and therefore the estimated minimum pressures of entrapment, do not change. Pressure estimates obtained from the MI indicate that plagioclase megacrysts from the Blanco transform fault are the product of crystallization in the upper mantle.

ACKNOWLEDGEMENTS

This project is supported by National Science Foundation grants EAR-1634206 and EAR-1634211. We are grateful for the help received at Virginia Tech from Lowell Moore and Natalie Sievers. We would like to thank David Neave and two anonymous reviewers, whose comments greatly improved the quality of this manuscript. In addition, discussions with and comments from David Graham and Adam Kent (Oregon State University) were also beneficial to this paper. Mark Biller's assistance with English editing was appreciated. Lastly, we thank Brian Monteleone (Woods Hole Oceanographic Institution) for assistance on the SIMS and help with data processing.

REFERENCES CITED

Bodnar, R.J., 2003, Reequilibration of fluid inclusions, *in* Samson, I., et al., eds., Fluid Inclusions: Analysis and Interpretation: Mineralogical Association of Canada Short Course 32, p. 213–230.

Brey, G., 1976, CO_2 solubility and solubility mechanisms in silicate melts at high pressures: Contributions to Mineralogy and Petrology, v. 57, p. 215–221, https://doi.org/10.1007/BF00405226.

Bryan, W.B., 1983, Systematics of modal phenocryst assemblages in submarine basalts: Petrologic implications: Contributions to Mineralogy and Petrology, v. 83, p. 62–74, https://doi.org/10.1007/BF00373080.

Christeson, G.L., Karson, J.A., and McIntosh, K.D., 2010, Mapping of seismic layer 2A/2B boundary above the sheeted dike unit at intermediate spreading crust exposed near the Blanco Transform: Geochemistry Geophysics Geosystems, v. 11, Q03015, https://doi.org/10.1029/2009GC002864.

Coumans, J.P., Stix, J., Clague, D.A., and Minarik, W.G., 2015, The magmatic architecture of Taney Seamount-A, NE Pacific Ocean: Journal of Petrology, v. 56, p. 1037–1067, https://doi.org/10.1093/petrology/egv027.

Dixon, J.E., Stolper, E.M., and Holloway, J.R., 1995, An experimental study of water and carbon dioxide solubilities in mid-ocean ridge basaltic liquids—Part I: Calibration and solubility models: Journal of Petrology, v. 36, p. 1607–1631, https://doi.org/10.1093/oxfordjournals.petrology.a037267.

Embley, R.W., and Wilson, D.S., 1992, Morphology of the Blanco transform fault zone-NE Pacific: Implications for its tectonic evolution: Marine Geophysical Researches, v. 14, p. 25–45, https://doi.org/10.1007/BF01674064.

Esposito, R., Hunter, J., Schiffbauer, J.D., Shimizu, N., and Bodnar, R.J., 2014, An assessment of the reliability of melt inclusions as recorders of the pre-eruptive volatile content of magmas: The American Mineralogist, v. 99, p. 976–998, https://doi.org/10.2138/am.2014.4574.

Gaetani, G.A., O'Leary, J.A., Shimizu, N., Bucholz, C.E., and Newville, M., 2012, Rapid reequilibration of H_2O and oxygen fugacity in olivine-hosted melt inclusions: Geology, v. 40, p. 915–918, https://doi.org/10.1130/G32992.1.

Hartley, M.E., Maclennan, J., Edmonds, M., and Thordarson, T., 2014, Reconstructing the deep CO_2 degassing behaviour of large basaltic fissure eruptions: Earth and Planetary Science Letters, v. 393, p. 120–131, https://doi.org/10.1016/j.epsl.2014.02.031.

Helo, C., Longpre, M.-A., Shimizu, N., Clague, D.A., and Stix, J., 2011, Explosive eruptions at mid-ocean ridges driven by CO_2-rich magmas: Nature Geoscience, v. 4, p. 260–263, https://doi.org/10.1038/ngeo1104.

Johnson, E.A., and Rossman, G.R., 2013, The diffusion behavior of hydrogen in plagioclase feldspar at 800–1000 °C: Implications for re-equilibration of hydroxyl in volcanic phenocrysts: The American Mineralogist, v. 98, p. 1779–1787, https://doi.org/10.2138/am.2013.4521.

Kent, A.J.R., 2008, Melt inclusions in basaltic and related volcanic rocks: Reviews in Mineralogy and Geochemistry, v. 69, p. 273–331, https://doi.org/10.2138/rmg.2008.69.8.

Kohut, E.J., and Nielsen, R.L., 2003, Low-pressure phase equilibria of anhydrous anorthite bearing mafic magmas: Geochemistry Geophysics Geosystems, v. 4, 1057, https://doi.org/10.1029/2002GC000451.

Kohut, E.J., and Nielsen, R.L., 2004, Melt inclusion formation mechanisms and compositional effects in high-An feldspar and high-Fo olivine in anhydrous mafic silicate liquids: Contributions to Mineralogy and Petrology, v. 147, p. 684–704, https://doi.org/10.1007/s00410-004-0576-0.

Koleszar, A.M., Saal, A.E., Hauri, E.H., Nagle, A.N., Liang, Y., and Kurz, M.D., 2009, The volatile contents of the Galapagos plume: Evidence for H_2O and F open system behavior in melt inclusions: Earth and Planetary Science Letters, v. 287, p. 442–452, https://doi.org/10.1016/j.epsl.2009.08.029.

Lange, A.E., Nielsen, R.L., Tepley, F.J., III, and Kent, A.J.R., 2013, The petrogenesis of plagioclase-phyric basalts at mid-ocean ridges: Geochemistry Geophysics Geosystems, v. 14, p. 3282–3296, https://doi.org/10.1002/ggge.20207.

Le Voyer, M., Kelley, K.A., Cottrell, E., and Hauri, E.H., 2017, Heterogeneity in mantle carbon content from CO_2-undersaturated basalts: Nature Communications, v. 8, 14062, https://doi.org/10.1038/ncomms14062.

Maclennan, J., 2017, Bubble formation and decrepitation control the CO_2 content of olivine-hosted melt inclusions: Geochemistry Geophysics Geosystems, v. 18, p. 597–616, https://doi.org/10.1002/2016GC006633.

McNutt, M., 1979, Compensation of oceanic tomography: An application of the response function technique to the Surveyor area: Journal of Geophysical Research, v. 84, p. 7589–7598, https://doi.org/10.1029/JB084iB13p07589.

Métrich, N., and Wallace, P.J., 2008, Volatile abundances in basaltic magmas and their degassing paths tracked by melt inclusions: Reviews in Mineralogy and Geochemistry, v. 69, p. 363–402, https://doi.org/10.2138/rmg.2008.69.10.

Michael, P.J., and Graham, D.W., 2015, The behavior and concentration of CO_2 in the suboceanic mantle: Inferences from undegassed ocean ridge and ocean island basalts: Lithos, v. 236–237, p. 338–351, https://doi.org/10.1016/j.lithos.2015.08.020.

Moore, G., 2008, Interpreting H_2O and CO_2 contents in melt inclusions: Constraints from solubility experiments and modeling: Reviews in Mineralogy and Geochemistry, v. 69, p. 333–362, https://doi.org/10.2138/rmg.2008.69.9.

Moore, R.L., Gazel, E., Tuohy, R., Lloyd, A.S., Esposito, R., Steele-MacInnis, M., Hauri, E.H., Wallace, P.J., Plank, T., and Bodnar, R.J., 2015, Bubbles matter: An assessment of the contribution of vapor bubbles to melt inclusion volatile budgets: The American Mineralogist, v. 100, p. 806–823, https://doi.org/10.2138/am-2015-5036.

Neave, D.A., Maclennan, J., Hartley, M.E., Edmonds, M., and Thordarson, T., 2014, Crystal storage and transfer in basaltic systems: The Skuggafjöll eruption, Iceland: Journal of Petrology, v. 55, p. 2311–2346, https://doi.org/10.1093/petrology/egu058.

Neave, D.A., Maclennan, J., Thordarson, T., and Hartley, M.E., 2015, The evolution and storage of primitive melts in the Eastern Volcanic Zone of Iceland: The 10 ka Grímsvötn tephra series (i.e. the Saksunarvatn ash): Contributions to Mineralogy and Petrology, v. 170, p. 21–28, https://doi.org/10.1007/s00410-015-1170-3.

Neave, D.A., Hartley, M.E., Maclennan, J., Edmonds, M., and Thordarson, T., 2017, Volatile and light lithophile elements in high-anorthite plagioclase-hosted melt inclusions from Iceland: Geochimica et Cosmochimica Acta, v. 205, p. 100–118, https://doi.org/10.1016/j.gca.2017.02.009.

Newman, S., and Lowenstern, J.B., 2002, VolatileCalc: A silicate melt–H_2O–CO_2 solution model written in Visual Basic Excel: Computers & Geosciences, v. 28, p. 597–604, https://doi.org/10.1016/S0098-3004(01)00081-4.

Schiavi, F., Provost, A., Schiano, P., and Cluzel, N., 2016, *P-V-T-X* evolution of olivine-hosted melt inclusions during high-temperature homogenization treatment: Geochimica et Cosmochimica Acta, v. 172, p. 1–21, https://doi.org/10.1016/j.gca.2015.09.025.

Steele-MacInnis, M., Esposito, R., and Bodnar, R.J., 2011, Thermodynamic model for the effect of post-entrapment crystallization on the H_2O-CO_2 systematics of volatile-saturated silicate melt inclusions: Journal of Petrology, v. 52, p. 2461–2482, https://doi.org/10.1093/petrology/egr052.

Wallace, P.J., and Carmichael, I.S.E., 1992, Sulfur speciation in submarine basaltic glasses as determined by measurements of S$K\alpha$ X-ray wavelength shifts: The American Mineralogist, v. 79, p. 161–167.

Wallace, P.J., Kamenetsky, V.S., and Cervantes, P., 2015, Melt inclusion CO_2 contents, pressures of olivine crystallization, and the problem of shrinkage bubbles: The American Mineralogist, v. 100, p. 787–794, https://doi.org/10.2138/am-2015-5029.

Wanless, V.D., and Behn, M.D., 2017, Spreading rate-dependent variations in crystallization along the global mid-ocean ridge system: Geochemistry Geophysics Geosystems, v. 18, p. 3016–3033, https://doi.org/10.1002/2017GC006924.

Wanless, V.D., and Shaw, A.S., 2012, Lower crustal crystallization and melt evolution at mid-ocean ridges: Nature Geoscience, v. 5, p. 651–655, https://doi.org/10.1038/ngeo1552.

Printed in USA